JOURNAL OF MATERIALS SCIENCE 20 (1985) 3191 – 3200

Electrical and optical properties of single crystalline α-Al_2O_3 doped with nickel

JOHN-SEA CHEN, F. A. KRÖGER
Department of Materials Science, University of Southern California, Los Angeles, California 90089-0241, USA

Nickel, substituting for aluminium in α-Al_2O_3 acts as an acceptor with a level ~ 2.46 eV above the conduction band if a large polaron model applies, $\cong 2.57$ eV $- H(\mu_h)$ above the band if a small polaron model applies. It is present as Ni^{3+} at high, and as Ni^{2+} at low, oxygen pressures, the concentration of Ni^{3+} being reduced to one-half of its high p_{O_2} value at $p_{O_2} = 1$ Pa. Analysis of the data provides proof that the native defect compensating the charge of Ni^{2+} ($=Ni'_{Al}$) is $V_O^{2\cdot}$, $Al_i^{3\cdot}$ being a minority species; $H_{F,Al} - 1/2H_S = 121$ kJ mol^{-1}.

1. Introduction

Owing to the high energy of formation of native defects, high-temperature properties of Al_2O_3 are invariably determined by the presence of impurities, in "pure" Al_2O_3 usually iron and magnesium. Even 1 ppm of impurities suffices to make the crystals extrinsic at 1600° C. Magnesium, iron and cobalt act as acceptors, titanium, silicon, hydrogen, yttrium and zirconium act as donors [1]. Nickel should act as an acceptor with a level somewhat below that of cobalt but above that of magnesium. Nickel occurs as Ni^{2+} and Ni^{3+}, occupying aluminium sites [2–5]. Ni^{2+} predominates at low, Ni^{3+} at high oxygen activities [6, 7]. $Al_2O_3:Ni^{2+}$ is colourless; $Al_2O_3:Ni^{3+}$ is yellow as a result of an absorption band with a maximum at 420 nm [6, 7]. This band was interpreted as a transfer transition [6, 8]. However, the poor agreement between the observed and the calculated peak position [8] and the agreement between the observed peak and the expected crystal field splitting (10 Dq = 3.04 eV [8]) suggest that it is still possible that the band is due to an internal transition in the Ni^{3+} ion. The ground state of Ni^{3+} ($3d^7$) is ^2E with a statistical weight $g_3 = 2 \times [\frac{1}{2}(2) + 1] = 4$; that of Ni^{2+} ($3d^8$) is $^3A_2$ with a weight $g_2 = (2 \times 1) + 1 = 3$ [4].

The present paper gives results for the electrical properties of $Al_2O_3:Ni$ at high temperatures and optical absorption of crystals cooled after a high-temperature anneal in atmospheres with different oxidizing power and interprets these results on the basis of a detailed point defect model.

2. Experimental techniques

A single crystal boule of α-Al_2O_3 grown from a melt containing 200 ppm Ni* ($=8.1 \times 10^{18}$ cm^{-3}) was put at our disposal.† Concentrations of nickel and impurities present in the sample were determined by semiquantitative spectrographic analysis. The results of the analysis, performed by a commercial establishment,‡ are presented in Table I. The nickel concentration is much lower than that of the melt from which the crystal was grown as a result of either evaporation or of a small distribution coefficient $k = c_s/c_l$, c_s and c_l being the concentrations of nickel in the solid and the liquid. A similar effect was observed for $Al_2O_3:Mg$ [9]. Several other elements are present in concentrations larger

*La Pierre Synthetique, Etablissements Baikowski, Annecy, Haute-Savoie, France.
†Courtesy Dr J. Smialek, NASA Lewis Research Center, Cleveland, Ohio, USA.
‡Pacific Spectrochemical Laboratories, Inc, 2558 Overland Avenue, Los Angeles, California 90062, USA.

0022–2461/85 $03.00 + .12

TABLE I Concentrations determined by semiquantitative spectrographic analysis

Element	Concentration	
	ppm by weight	cm^{-3} ($\times 10^{-17}$)
Ni	6.6	2.68
Mg	12.0	11.8
Fe	19.0	8.1
Si	250.0	212.0
Ca	8.6	5.1
Cu	1.0	0.38

than that of nickel. This is disturbing, since some of them (e.g. magnesium and iron) are known to be acceptors, whereas others (e.g. silicon) are known to act as donors.

The large value reported for silicon is probably not reliable [10] but a smaller amount of silicon may be present. Despite the presence of these impurities, it is still possible to obtain meaningful results concerning the activity of nickel in the crystal.

Plates of $\cong 1.6$ mm thick, with the plane of the samples $\perp c$, were cut for the electrical measurements. Plates of 3.43 mm thick with the same orientation were cut for the optical absorption measurements. The latter were polished for optical flatness with diamond paste down to 1 μm. D.c. electrical conductivity $\sigma \parallel c$ and the emf of an oxygen concentration cell with the sample as the electrolyte were measured as $f(T, p_{O_2})$ by a three-contact method, a volume guard being used to eliminate surface and gas phase conduction as described in [11]. Ionic transference numbers $t_i = \sigma_i/\sigma$ were determined as $f(T, p_{O_2})$ by differentiating the emf of the concentration cells. Oxygen pressures were established by pure oxygen, air and mixtures of CO/CO_2. Optical absorption $\parallel c$ was measured with a double beam spectrophotometer.§

3. Experimental results

Fig. 1 shows conductivity as a function of

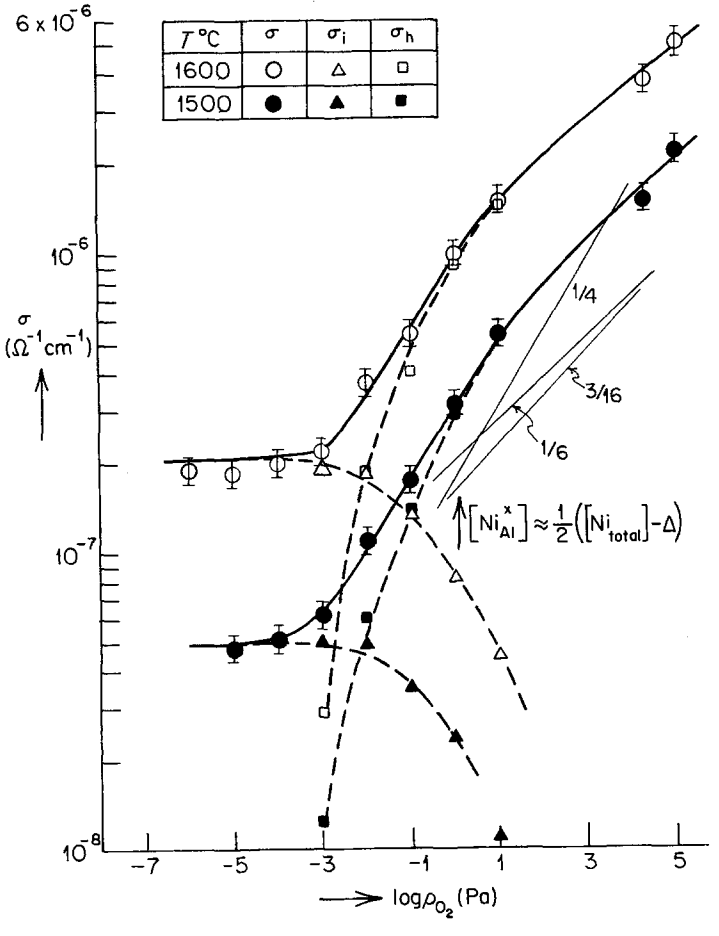

Figure 1 D.c. conductivity as $f(p_{O_2})$ at 1500 and 1600° C and the partial ionic and electronic conductivities $\sigma_i = t_i\sigma$ and $\sigma_{el} \equiv \sigma_h = \sigma(1 - t_i)$ using the t_i values of Fig. 2.

§Beckman, Fullerton, California, "Acta M-6".

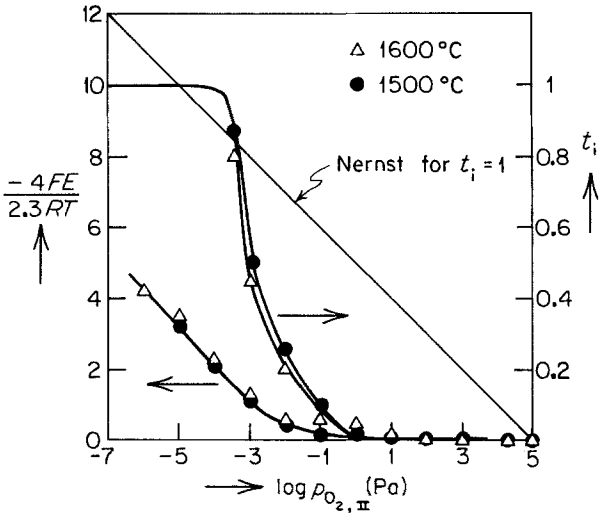

Figure 2 EMF of an oxygen concentration cell $Pt,p_{O_{2,I}}|Al_2O_3:Ni|Pt,p_{O_{2,II}}$ and t_i calculated from

$$(t_i)p_{O_{2,II}} = \left[\frac{\partial\,(4FE/2.3RT)}{\partial \log (p_{O_{II,2}})}\right]_{p_{O_{2,I}}}$$

oxygen pressure at 1500 and 1600° C and the partial ionic and electronic conductivities $\sigma_i = \sigma t_i$ and $\sigma_{el} = \sigma(1 - t_i)$, using the ionic transference numbers t_i obtained from the emf measurements shown in Fig. 2. The fact that σ_{el} increases with oxygen pressure shows that we are dealing with holes: $\sigma_{el} = \sigma_h$ and the material is acceptor dominated. Fig. 3 shows conductivity at four oxygen pressures as a function of temperature, measured with slow or fast temperature changes. In the former case equilibrium in the crystal and between the crystal and the

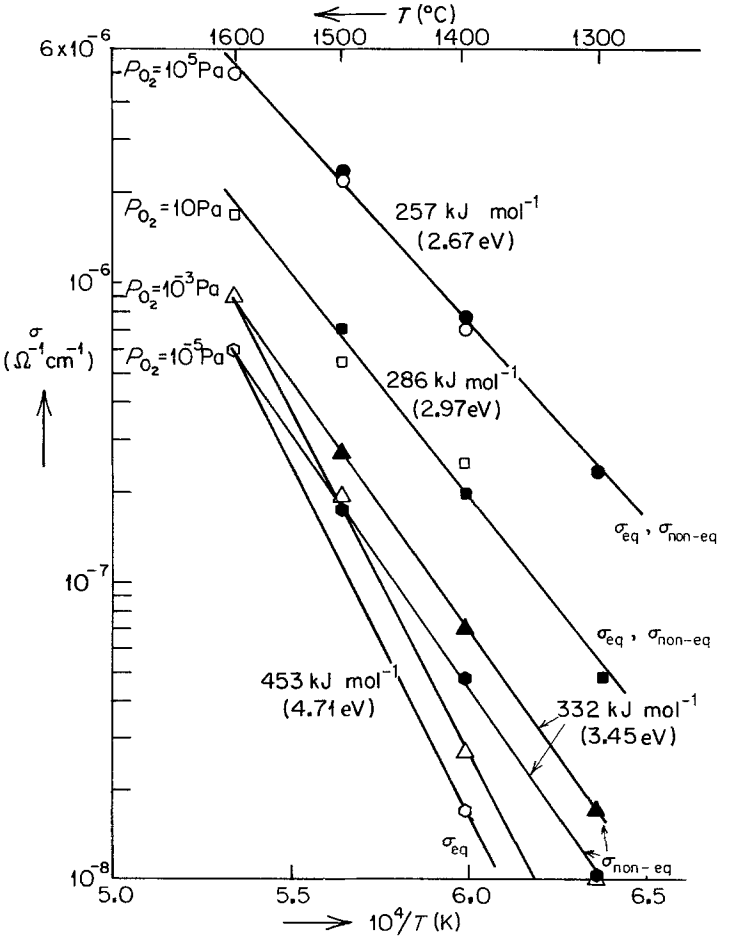

Figure 3 Temperature dependence at four oxygen pressures of conductivity with maintenance of equilibrium (open symbols) or under conditions that equilibrium is not maintained (solid symbols).

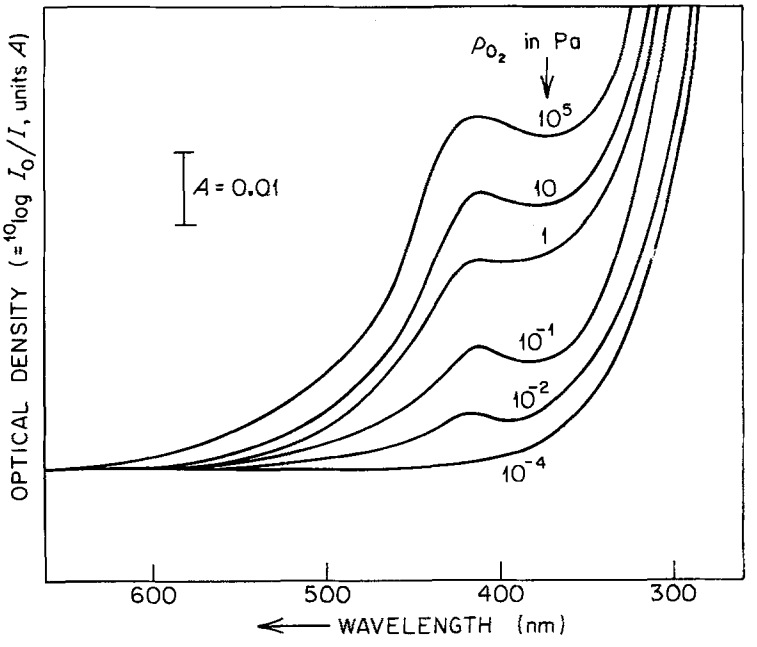

Figure 4 Optical density at room temperature as a function of wavelength of crystals annealed at 1500° C under various oxygen pressures.

atmosphere is maintained (open symbols; equilibration time at the lowest temperature ≅ 24 h). With rapid variation of temperature, equilibrium was not maintained (solid symbols; typical cooling times from 1600 to 1400° C 5 min). The conductivities are represented by

$$\sigma(10^5\,\mathrm{Pa})_{\text{eq and non-eq}} = 109 \times \exp(-257\,\mathrm{kJ\,mol^{-1}}/RT)\,\Omega^{-1}\,\mathrm{cm^{-1}} \quad (1)$$

$$\sigma(10\,\mathrm{Pa})_{\text{eq and non-eq}} = 224 \times \exp(-286\,\mathrm{kJ\,mol^{-1}}/RT)\,\Omega^{-1}\,\mathrm{cm^{-1}} \quad (2)$$

$$\sigma(10^{-3}\,\mathrm{Pa})_{\text{eq}} = 8 \times 10^6 \times \exp(-453\,\mathrm{kJ\,mol^{-1}}/RT)\,\Omega^{-1}\,\mathrm{cm^{-1}} \quad (3)$$

$$\sigma(10^{-3}\,\mathrm{Pa})_{\text{non-eq}} = 2.6 \times 10^3 \times \exp(-332\,\mathrm{kJ\,mol^{-1}}/RT)\,\Omega^{-1}\,\mathrm{cm^{-1}} \quad (4)$$

$$\sigma(10^{-5}\,\mathrm{Pa})_{\text{eq}} = 5.3 \times 10^6 \times \exp(-453\,\mathrm{kJ\,mol^{-1}}/RT)\,\Omega^{-1}\,\mathrm{cm^{-1}} \quad (5)$$

$$\sigma(10^{-5}\,\mathrm{Pa})_{\text{non-eq}} = 1.7 \times 10^3 \times \exp(-332\,\mathrm{kJ\,mol^{-1}}/RT)\,\Omega^{-1}\,\mathrm{cm^{-1}} \quad (6)$$

There is practically no difference between the results for equilibrium and non-equilibrium at $p_{O_2} \geqslant 10$ Pa where the conductivity is due to holes, but there is a marked difference at $p_{O_2} \leqslant 10^{-3}$ Pa where the conductivity is mainly ionic.

Optical absorption spectra at room temperature of crystals annealed for 60 h at 1600° C are shown in Fig. 4. The spectra show a peak with Gaussian shape with maximum at $2.38 \times 10^4\,\mathrm{cm^{-1}} = 2.95\,\mathrm{eV}$ and a half-width of $7400\,\mathrm{cm^{-1}}$, and the beginning of a stronger band at shorter wavelength. There is no sign of a peak due to Mg^x_{Al} as found in oxidized Al_2O_3: Mg [9]. The observed peak is responsible for the yellow colour of the oxidized samples and is no doubt identical with the band reported by earlier workers [6–8]. Its intensity decreases with decreasing oxygen pressure reaching half intensity at $p_{O_2} \cong 1$ Pa; the band disappears altogether at $p_{O_2} < 10^3$ Pa (Fig. 5). The absorption saturates at $p_{O_2} \geqslant 10^3$ Pa. Since the absorption band is due to Ni^{3+}, this result indicates that at these oxygen pressures the Ni^{3+} concentration reaches a saturation value.

4. Discussion

The variation in the intensity of the band responsible for the yellow colour of the sample results from a variation in the position of the Fermi level. Since the variability of the Fermi level by oxidation–reduction is relatively limited in scope, the observed colour change and the absence of an absorption band due to Mg^x_{Al} indicate that in spite of the presence of other donors and acceptors, the Fermi level remains close to the Ni'_{Al} level. The Mg'_{Al} level (which lies closer to the valence band) remains always

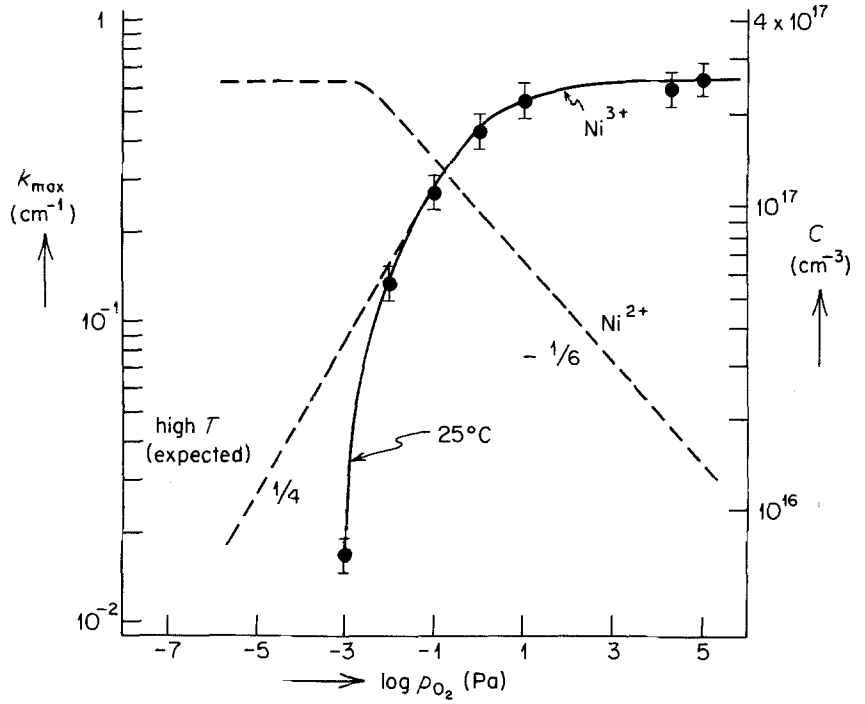

Figure 5 The absorption coefficient at the maximum, $\lambda = 420$ nm, at room temperature, the corresponding concentration of Ni^{3+}, and that of $Ni^{2+} = [Ni]_{total} - [Ni^{3+}]$, for samples annealed at 1500° C under various oxygen pressures.

occupied, and the Fe'_{Al} level (which is expected to be above the Ni'_{Al} level) remains mostly empty; iron is present primarily as Fe^{3+}, with possibly some Fe^{4+}. This is possible when a sufficient amount of donors (Fe^{x}_{Al} or Si^{x}_{Al}) are present which, after ionization to $Fe^{\cdot}_{Al}$ and $Si^{\cdot}_{Al}$ compensate Mg'_{Al}.

The isotherms of Fig. 1 show that the material is acceptor dominated. Since the Fermi level is close to the Ni'_{Al} level, it indicates that Ni_{Al} is an acceptor. The main defects compensating for Ni'_{Al} and Mg'_{Al} are the ionized foreign donors D ($Fe^{\cdot}_{Al}$ and $Si^{\cdot}_{Al}$) and the native defects $V_O^{2\cdot}$ or $Al_i^{3\cdot}$:

$$[D^{\cdot}] - [Mg'_{Al}] + 2[V_O^{2\cdot}] + 3[Al_i^{3\cdot}] \cong [Ni'_{Al}]$$

A variation in $[Ni'_{Al}]$ with oxygen pressure with formation of Ni^{x}_{Al} involves the native defects $V_O^{2\cdot}$ and/or $Al_i^{3\cdot}$. The shape of the isotherms for σ_i and σ_h depend on the magnitude of $[D^{\cdot}] - [Mg'_{Al}]$ [12]. For $[D^{\cdot}] - [Mg'_{Al}] < 0$, the Fermi level is close to the Mg'_{Al} level and no oxidation–reduction of Ni_{Al} is to be expected. This possibility can be excluded. For $[D^{\cdot}] - [Mg'_{Al}] > 0$ a fixed amount of Ni'_{Al}, $[Ni'_{Al}] \cong [D^{\cdot}] - [Mg'_{Al}]$ will be present at all p_{O_2}. This still allows oxidation–reduction of Ni_{Al} if the fixed concentration is $< [Ni]_{total}$, the amount that can be oxidized or reduced being equal to $\Delta = [Ni]_{total} - ([D^{\cdot}] - [Mg'_{Al}])$. For $\Delta < \frac{1}{2}[Ni]_{total}$, we expect practically constant concentrations of Ni^{2+} and Ni^{3+} at large p_{O_2}, and therefore $[h^{\cdot}]$ and $\sigma_h \propto [h^{\cdot}]$ constant with a value determined by

$$K_a^{Ni} = \frac{[Ni'_{Al}][h^{\cdot}]}{[Ni^{x}_{Al}]} \qquad (7)$$

This saturation, demonstrated for a model with $[Al_i^{3\cdot}] \gg [V_O^{2\cdot}]$, in Fig. 6a is not in agreement with the isotherms of Fig. 1 which show σ_h to be dependent on p_{O_2} at all p_{O_2}. Only for $0 < \Delta < \frac{1}{2}[Ni]_{total}$ can one expect a variation of σ_h with p_{O_2}. This situation is demonstrated in Fig. 6b for the case where $[V_O^{2\cdot}] \gg [Al_i^{3\cdot}]$. The same situation can of course occur for the model with $[Al_i^{3\cdot}] \gg [V_O^{2\cdot}]$. The variation of σ_h with p_{O_2} is limited to ranges I and II where $[Ni'_{Al}] > \Delta$; in range III where $[Ni'_{Al}] \cong \Delta$, $[h^{\cdot}]$ is independent of p_{O_2}. The fact that a high p_{O_2} range with constant σ_h is not observed indicates that $\Delta \ll ([Ni]_{total} - \Delta)$ or $\Delta \ll \frac{1}{2}[Ni]_{total}$, i.e. $[D^{\cdot}] \cong 1.2 \times 10^{18}\ cm^{-3}$. The slopes of $\sigma_h \propto [h^{\cdot}] \propto p_{O_2}^{n}$ with $n = 1/6$ and $3/16$ for $[V_O^{2\cdot}] \gg$ or $\ll [Al_i^{3\cdot}]$ respectively (for $\Delta \cong 0$) are too close to decide between these two possibilities on this basis: both fit the experimental data of Fig. 1 reasonably well. The data also show a change in slope

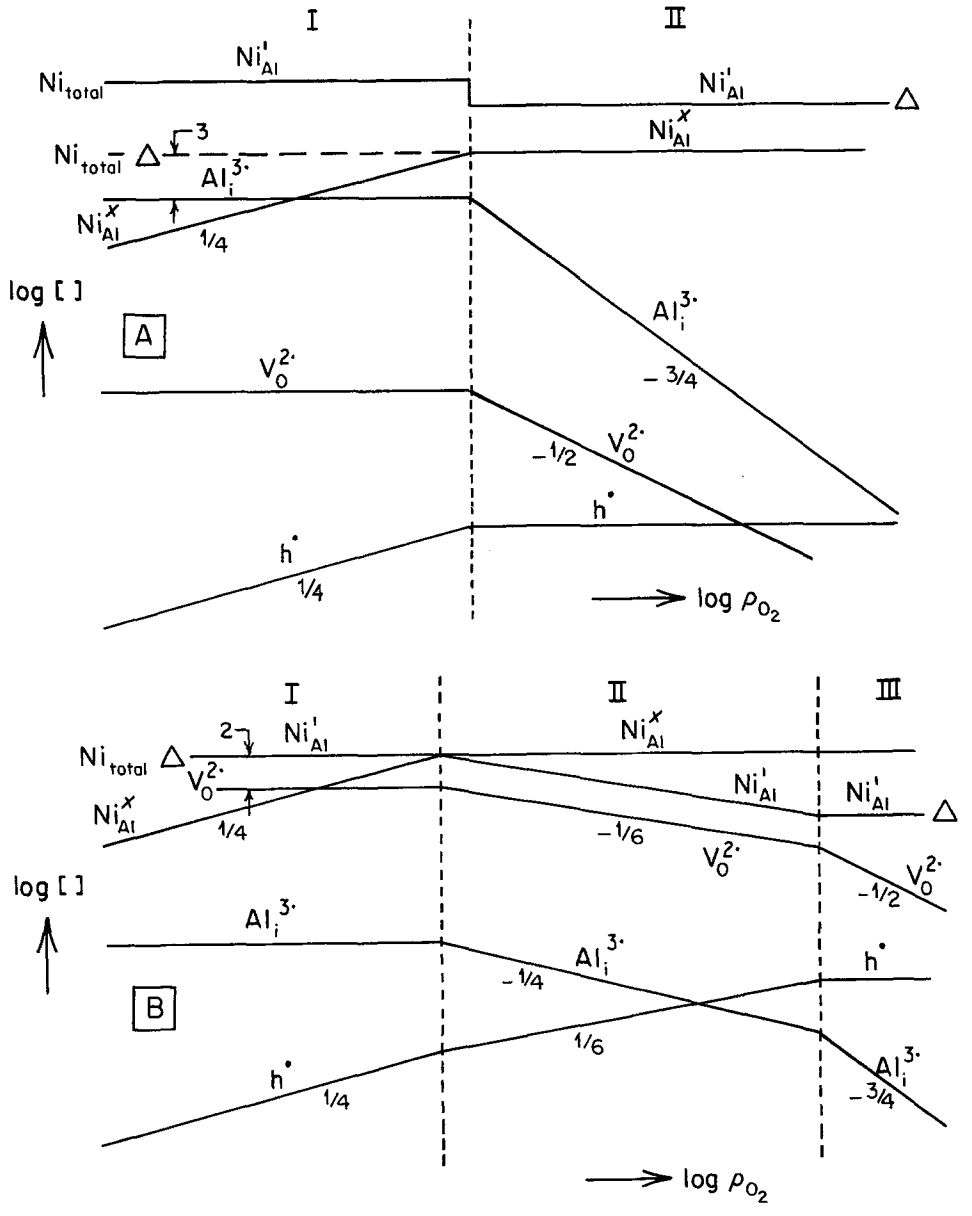

Figure 6 Approximate defect concentration isotherms for models dominated by $[Ni'_{Al}] \cong 3[Al_i^{3\cdot}]$ with $\Delta > \frac{1}{2}[Ni]_{total}$ (A), and $[Ni'_{Al}] \cong 2[V_O^{2\cdot}]$ with $\Delta < \frac{1}{2}[Ni]_{total}$ (B).

at $p_{O_2} \cong 1$ Pa corresponding to the change from $n = 1/6$ or $3/16$ to $1/4$ expected for the models. The larger slopes observed at $p_{O_2} < 10^{-2}$ Pa are not predicted by the model; they are probably incorrect, originating from the low accuracy of the emf values and the corresponding t_i and t_h values in this region. The isotherms at low p_{O_2} where $\sigma \cong \sigma_i$ also are described equally well by both models. A choice can be made between the two models on the basis of the observed variation of σ_i with temperature at low p_{O_2} which show a marked difference in the activation energy for conductivity measured with maintenance of equilibrium, σ_{eq}, and conductivity measured under conditions where equilibrium is not maintained, $\sigma_{non\text{-}eq}$ (Fig. 3 and Equations 5 and 6).

Since $[V_O^{2\cdot}]$ and $[Al_i^{3\cdot}]$ are both independent of p_{O_2}, the difference between equilibrium and non-equilibrium cannot be due to the freezing of the oxygen uptake or evolution, but must be due to the blocking of internal processes. For the model dominated by $Al_i^{3\cdot}$, $[Al_i^{3\cdot}] = 1/3([Ni']_{total} - \Delta)$ = constant, but $[Al_i^{3\cdot}]$ which regulates σ_i is

determined by the Schottky and Frenkel disorder reactions:

$$0 \rightarrow 2V_{Al}^{3'} + 3V_O^{2\cdot}$$

$$[V_{Al}^{3'}]^2[V_O^{2\cdot}]^3 = K_S \quad (8)$$

$$Al_{Al}^{x} + V_i^{x} \rightarrow Al_i^{3\cdot} + V_{Al}^{3'}$$

$$[V_{Al}^{3'}][Al_i^{3\cdot}] = K_{F,Al} \quad (9)$$

Either of these reactions or both of them may be frozen in. If both reactions reach equilibrium while $2[V_O^{2\cdot}] \cong [Ni'_{Al}] \cong ([Ni]_{total} - \Delta) \cong [Ni]_{total}$, $\sigma_i = \sigma_{i,eq} = 1.06 \times q\mu_{Al}NK_{F,Al}K_S^{-1/2}[Ni]_{total}^{3/2}$ with an activation energy $H(\mu_{Al}) + H_{F,Al} - 1/2H_S$. Square brackets indicate concentrations per molecule Al_2O_3; $N = 2.34 \times 10^{22}\,cm^{-3}$, the number of molecules Al_2O_3 per cm^3. When Reaction 8 is frozen in but Reaction 9 is not, $[V_{Al}^{3'}]$ is constant at its 1600° C value:

$$[V_{Al}^{3'}]_{1600} = 2^{3/2}(K_{S,1600})^{1/2}[Ni]_{total}^{-3/2}$$

and

$$\sigma_{i,\,non\text{-}eq(8)} \propto \mu_{Al}K_{F,Al}[V_{Al}^{3'}]_{1600}^{-1} \quad (11)$$

with an activation energy $H(\mu_{Al}) + H_{F,Al}$. On the other hand, when Reaction 8 reaches equilibrium but Reaction 9 does not, $[V_{Al}^{3'}]$ reaches its equilibrium value, but, since Reaction 9 is frozen, this does not affect $[Al_i^{3\cdot}]$. Hence $[Al_i^{3\cdot}] = [Al_i^{3\cdot}]_{1600}$ = constant and the activation energy of $\sigma_{i,\,non\text{-}eq(9)}$ is $H(\mu_{Al})$. The same result is found when both Reactions 8 and 9 are frozen in.

Thus there are two possible expressions for the differences in the activation energies under equilibrium and non-equilibrium conditions. When Reaction 8 is frozen in,

$$H_{eq} - H_{non\text{-}eq} = -\tfrac{1}{2}H_S \quad (12)$$

When Reaction 9 or 8 and 9 are frozen in,

$$H_{eq} - H_{non\text{-}eq} = H_{F,Al} - \tfrac{1}{2}H_S \quad (13)$$

Since $H_{eq} - H_{non\text{-}eq} = (453\text{–}332)\,kJ\,mol^{-1} = 121\,kJ\,mol^{-1} > 0$ while $H_s > 0$, Possibility 12 has been rejected. Possibility 13, however, is acceptable if $H_{F,Al} - \frac{1}{2}H_S \cong 121\,kJ\,mol^{-1}$.

Values for these parameters have been calculated by Dienes *et al.* [13] and Catlow *et al.* [14], the last authors giving results based on empirical and non-empirical potentials respectively. The results by Catlow *et al.* are considered the most reliable. Table II compares their results with the observed energy difference.

TABLE II Enthalpies (kJ mol^{-1})

Source	$H_{F,Al}$	H_S	$H_{F,Al} - \frac{1}{2}H_S$
Dienes *et al.* [13]	1920	2750	545
Catlow *et al.* [14]	1004–	2010–	0–116
(empirical potentials)	1246	2260	
Catlow *et al.* [14]	1364	2475	126.5
(non-empirical potentials)			
$\sigma_{eq}/\sigma_{non\text{-}eq}$			121

There is good agreement between the observed difference and the values calculated by Catlow *et al.* [14]; the ones obtained using non-empirical potentials and the largest values arrived at by using empirical potentials are equally acceptable. This agreement supports the proposed model. While the proposed model involves isolated point defects, an alternative explanation involving pairing should also be considered. Two types of pairs may be formed:

$$Ni'_{Al} + V_O^{2\cdot} \rightarrow (Ni_{Al}V_O)^{\cdot}; \; K_{P,V(O)} \quad (14)$$

and

$$Ni'_{Al} + Al_i^{3\cdot} \rightarrow (Ni_{Al}Al_i)^{2\cdot}; \; K_{P,Al(i)} \quad (15)$$

For approach distances $r \cong 0.19\,nm$, $H_{P,V(O)} \cong -2q^2/\varepsilon r$ and $H_{P,Al(i)} \cong -3q^2/\varepsilon r$ with $\varepsilon \cong 10$, the pairing constants are expected to be $K_{P,V(O)} = 4 \exp 144\,kJ\,mol^{-1}/RT$ and $K_{P,Al(i)} = 2 \exp 213\,kJ\,mol^{-1}/RT$ respectively. With these constants and the nickel concentration as present in the sample, no appreciable pairing is expected for the $V_O^{2\cdot}$ model at $T \geqslant 1520°\,C$. For the $Al_i^{3\cdot}$ model, where pairing should occur, the model gives a difference $H_{eq} - H_{noneq\text{-}eq} = H_{P,Al(i)} = 213\,kJ\,mol^{-1}$, about twice the observed value. Therefore both these explanations have to be rejected. The accepted explanation remains the one based on the $V_O^{2\cdot}$ model with freezing in of the Frenkel disorder reaction, with or without freezing in of the Schottky disorder reaction. It may seem surprising that freezing of the Frenkel disorder process occurs. It should be noted, however, that when the temperature is decreased, this reaction should run to the right, involving an activation energy $> H_{F,Al}$. This is the first time that there is evidence for the freezing in of a disorder process and its effect on the difference between σ_{eq} and $\sigma_{non\text{-}eq}$. Previously such effects were always attributed to the blocking of oxygen uptake or release. Evidently, freezing in of the internal processes may also have occurred there. Therefore, earlier interpretations based

exclusively on the blocking of oxygen exchange should be considered with caution and corrections should be made when called for.

According to Equation 10, the values of $\sigma_{i,eq}$ for acceptor dominated materials at low p_{O_2} should be proportional to the acceptor concentration to the power 3/2. Applying this relation to the present sample (with $\sigma_{i,eq}$ at 1600° C equal to $2 \times 10^{-7}\,\Omega^{-1}\,cm^{-1}$), to Al_2O_3:Mg [9] with $N[Mg] = 8 \times 10^{17}\,cm^{-3}$, $\sigma_{i,eq} = 3.8 \times 10^{-5} \simeq^{-1} cm^{-1}$, and to Al_2O_3:Co [15] with $N[Co] = 10^{18}\,cm^{-3}$, $\sigma_{i,eq} = 2 \times 10^{-5}\,\Omega^{-1}\,cm^{-1}$ leads to an active nickel concentration $N[Ni] = 2.42 \times 10^{16}\,cm^{-3}$ and $4.65 \times 10^{16}\,cm^{-3}$, respectively, 10 to 5 times smaller than the value of $2.7 \times 10^{17}\,cm^{-3}$ determined by spectrochemical analysis (Table I), indicating that either the analysis is incorrect or that only a fraction of the nickel is active as acceptor. The discrepancy is indeed somewhat reduced by introducing compensation: For $\Delta = 10^{17}\,cm^{-3}$, $N[Ni] = 1.7 \times 10^{17}\,cm^{-3}$, and the discrepancy factor is reduced to 7 or 4. Stronger compensation would cause a change in the expected isotherm shapes and is not acceptable. Therefore either the concentration of dopants in the earlier papers, or that assumed in the present work are in error.

Combining Equations 5 and 1, remembering that $K_{F,Al}$ and K_S depend exponentially on T^{-1} with $H_{F,Al} - \frac{1}{2}H_S = 121\,kJ\,mol^{-1}$ and pre-exponentials $K^0_{F,Al}$ and K^0_S, taking $\Delta = 0$, leads to an expression for the mobility of $Al_i^{3\cdot}$:

$$(\mu_{Al})_{\parallel c} = 3.4 \times 10^{-5} K_S^{0\frac{1}{2}} (K^0_{F,Al})^{-1} \times \exp(-332\,kJ\,mol^{-1}/RT) \quad (16)$$

The activation energy of $332\,kJ\,mol^{-1}$ ($=3.45\,eV$) agrees well with an earlier experimental value [9] if the latter is corrected with $(H_{F,Al} - \frac{1}{2}H_S)$ to $(H(\mu_{Al})_{\parallel c} = 3.45\,kJ\,mol^{-1}$ ($=3.59\,eV$). It is somewhat smaller than a value $447\,kJ\,mol^{-1}$ ($=4.65\,eV$) computed by Dienes *et al.* [13]. The value of the pre-exponential remains uncertain because $K^0_{F,Al}$ and K^0_S are unknown.

Let us now turn to σ_h, dominating the conductivity at high p_{O_2}. As we saw earlier, the p_{O_2} dependence is reasonably accounted for by the $V_O^{2\cdot}$ dominated model (Fig. 6b) which we believe to be the correct one. In view of the p_{O_2} dependence of σ_h, differences between $\sigma_{h,eq}$ and $\sigma_{h,non\text{-}eq}$ should be expected as a result of blocking of the oxygen exchange between the sample and the atmosphere; the disorder processes affecting the behaviour of σ_i at low p_{O_2} do not play a role here. For the $V_O^{2\cdot}$ model, oxidation is described by

$$\tfrac{1}{2}O_2(g) + V_O^{2\cdot} + 2Ni'_{Al} \rightleftarrows O_O^x + Ni^x_{Al} \quad (17)$$

with

$$K^{Ni}_{ox,V} = \frac{[Ni^x_{Al}]^2}{[Ni'_{Al}]^2[V_O^{2\cdot}]}\, p_{O_2}^{-\frac{1}{2}} \quad (18)$$

At high p_{O_2} and $\Delta \cong 0$, $[Ni^x_{Al}] \cong [Ni]_{total}$ and under equilibrium conditions

$$[Ni'_{Al}] \cong 2[V_O^{2\cdot}] = 2^{1/3}(K^{Ni}_{ox,V})^{-1/3}[Ni]^{2/3}_{total}\, p_{O_2}^{-1/6} \quad (19)$$

Ionization of Ni^{3+} produces holes:

$$Ni^x_{Al} \rightarrow Ni'_{Al} + h^{\cdot}, \quad K^{Ni}_a = \frac{[h^{\cdot}][Ni'_{Al}]}{[Ni^x_{Al}]} \quad (20)$$

Thus for complete equilibrium

$$\sigma_{h,eq} = \mu_h q[h^{\cdot}]N = 2^{-1/3}\mu_h qNK^{Ni}_a(K^{Ni}_{ox,V})^{1/3}[Ni]^{1/3}_{total}\, p_{O_2}^{1/6} \quad (21)$$

with an activation energy of $H(\mu_h) + E^{Ni}_a + 1/3H^{Ni}_{ox,V}$.

When equilibrium with the atmosphere is frozen, the oxygen content of the sample remains fixed and $[V_O^{2\cdot}]$ = constant = $[V_O^{2\cdot}]_{1600}$. In this case $[h^{\cdot}]$ varies only as a result of Reaction 20 with an expected activation energy of $H(\mu_h) + E^{Ni}_a$. The observed equality of $\sigma_{h,eq}$ and $\sigma_{h,non\text{-}eq}$ therefore indicates that $H^{Ni}_{ox,V} \cong 0$. Reaction 17 is a combination of

$$\tfrac{1}{2}O_2(g) + V_O^{2\cdot} \rightarrow O_O^x + 2h^{\cdot}, \quad K_{ox,V(O)} \quad (22)$$

and twice Reaction 20.

Therefore

$$K^{Ni}_{ox,V} \equiv K_{ox,V(O)}(K^{Ni}_a)^{-2}$$

or

$$H^{Ni}_{ox,V} = H_{ox,V(O)} - 2E^{Ni}_a = 0.$$

Or, since

$$H^{Ni}_{ox,V} \cong 0, \quad H_{ox,V(O)} = 2E^{Ni}_a.$$

According to Equation 1 and Fig. 3, the activation energy of σ_h is $257\,kJ\,mol^{-1}$. Identification of this value with $H(\mu_h) + E^{Ni}_a$ taking $H(\mu_h) \cong 0$ (as is acceptable if the holes are large polarons) gives $E^{Ni}_a = 257\,kJ\,mol^{-1}$ ($=2.67\,eV$) and $H_{ox,V(O)} = 2E^{Ni}_a = 514\,kJ\,mol^{-1}$ ($=5.34\,eV$).

For a large polaron model with statistical weights of Ni^{3+} and Ni^{2+} of 4 and 3 respectively

$$(K_a^{Ni})_{lp} = \frac{8}{3}\left(\frac{2\pi m_h^* kT}{h^2}\right)^{3/2} N \times \exp - (E_{Ni'} - E_v)/kT \quad (23)$$

and thus

$$E_a^{Ni} \equiv \tfrac{3}{2}kT + (E_{Ni'} - E_v).$$

For $T \cong 1073\,K$, $T \cong 4.5 \times 10^3 \exp - 13.9\ kJ\,mol^{-1}$, $kT \cong 13.9\,kJ\,mol^{-1}$ ($=0.14\,eV$) and thus the separation of the Ni'_{Al} level and the edge of the valence band, $(E_{Ni'} - E_v) \cong 236\,kJ\,mol^{-1}$ ($=2.46\,eV$). This value is somewhat smaller than that observed for cobalt (3.06 eV) and close to the anticipated value (2 eV) [16].

The value found for $H_{ox,V(O)} = 514\,kJ\,mol^{-1}$ (5.39 eV) is to be compared with an earlier experimental value of $390\,kJ\,mol^{-1}$ ($4.05\,eV \equiv 2.15\,eV + 3800\beta_{Fe}$) [17] and with values computed by Catlow *et al* [14] of $\frac{1}{2}E_{O_2} = 426\,kJ\,mol^{-1}$ ($=4.43\,eV$) when using non-empirical potentials, and of $193\,kJ\,mol^{-1}$ (2.0 eV) when using empirical potentials. Another estimate of $H_{ox,V(O)}$ can be obtained from the observation that the p_{O_2} dependence of t_i is virtually independent of temperature (Fig. 2). According to its definition, $t_i = \frac{1}{2}$ when $\sigma_i = \sigma_h$ or $3q[Al_i^{3\cdot}]\mu_{Al} = q[h^{\cdot}]\mu_h$. This point is reached at $p_{O_2} = 10^{-2}$ Pa which according to Fig. 5 lies in the low p_{O_2} range where $[Ni'_{Al}] \cong [Ni]_{total}$. In this range $\sigma_{i,eq}$ is described by Equation 10. An expression for $\sigma_{h,eq}$ is obtained by combining Equation 22 with $[V_O^{2\cdot}] = \frac{1}{2}[Ni'_{Al}] = \frac{1}{2}[Ni]_{total}$ with $\sigma_{h,eq} = c_h q\mu_h$:

$$\sigma_h = 2^{-1/2} q\mu_h N[Ni]_{total}^{1/2} K_{ox,V(O)}^{1/2} p_{O_2}^{1/4} \quad (24)$$

The temperature dependences of $\sigma_{i,eq}$ and $\sigma_{h,eq}$ are equal if

$$H(\mu_{Al}) + H_{F,Al} - \tfrac{1}{2}H_S = H(\mu_h) + \tfrac{1}{2}H_{ox,V(O)}$$

Use of the values arrived at for the enthalpies at the left-hand side, taking $H(\mu_h) = 0$ leads to $H_{ox,V(O)} = 906\,kJ\,mol^{-1}$ ($=9.4\,eV$), a value much larger than the one arrived at before. Introducing a temperature dependence for μ_h, e.g. $H(\mu_h) = 100\,kJ\,mol^{-1}$ ($\cong 1\,eV$) which would be acceptable should holes behave as small polarons, would reduce the value arrived at to $\cong 700\,kJ\,mol^{-1}$, closer to the one of $514\,kJ\,mol^{-1}$ found earlier. This would reduce the value for $E_{Ni} - E_v$ arrived at earlier to $257 - H(\mu_h) = 157\,kJ\,mol^{-1}$ ($=1.63\,eV$) a value still close to the anticipated value of 2 eV [16]. A smaller $H(\mu_h)$ would of course give a correspondingly larger value for $E_{Ni} - E_v$.

The optical data of Fig. 5 allow us to obtain values of $[Ni_{Al}^x]$ and $[Ni'_{Al}]$ as a function of p_{O_2}. (e.g. for $p_{O_2} = 10^5$ Pa, assuming $\Delta \cong 0$, $[Ni_{Al}^x] = [Ni]_{total} = 2.7 \times 10^{17}\,cm^{-3}/N$, $[Ni'_{Al}] = 1.5 \times 10^{16}\,cm^{-3}/N$ and $[Ni^x]/[Ni'_{Al}] = 18$.) Introducing this value in Equation 20, using Equation 23 for K_a^{Ni} valid for the large polaron model leads to

$$N[h^{\cdot}]_{1500°,10^5\,Pa} = 18N(K_a^{Ni})_{lp} = 48\left(\frac{2\pi m_h^* k}{h^2}\right)^{3/2} T^{3/2} \times \exp - (E_{Ni} - E_v)/kT$$

which for $m_h^* \cong m$, the rest mass of the electron, and $E_a^{Ni} = 3/2kT + (E_{Ni} - E_v)$ gives

$$\sigma_h = N[h^{\cdot}]q\mu_h = 5.6 \times 10^3\,\mu_h \times \exp(-E_a^{Ni}/kT)\Omega^{-1}\,cm^{-1}.$$

Equating this expression with the values observed under the same conditions, $\sigma_h = 2 \times 10^{-6}\,\Omega^{-1}\,cm^{-1}$, and using for E_a^{Ni} the value arrived at earlier, leads to

$$(\mu_h)_{lp,1500°} = 1.4 \times 10^{-2}\,V^{-1}\,sec^{-1}$$

Earlier reported values vary from 10^4 to $6 \times 10^{-3}\,cm^2\,V^{-1}\,sec^{-1}$ [16]; in [9] a thermally activated μ_h was arrived at (which does not fit the large polaron model). For the small polaron model with holes moving via O^{2-} ions, on the other hand, $N(K_a^{Ni})_{sp} = 3N \exp - E_a^{Ni}/kT$ with $E_a^{Ni} \equiv (E_{Ni'} - E_v) = 257\,kJ\,mol^{-1} - H(\mu_h) \cong 157\,kJ\,mol^{-1}$, leading to $N[h^{\cdot}]_{1500°,10^5\,Pa} = 18N(K_a^{Ni})_{sp} = 2.93 \times 10^9\,cm^{-3}$ and $(\mu_h)_{sp,1500°} = 4.3 \times 10^{-7}\,cm^2\,V^{-1}\,sec^{-1}$ or $(\mu_h)_{sp} = 3.8 \times 10^{-4} \exp(-100\,kJ\,mol^{-1}/RT)$.

For bands with a Gaussian shape, the absorption coefficient at the maximum is related to the concentration of absorbing centres c by the formula [18]

$$\frac{c}{cm^{-3}} = 1.08 \times 10^{13} \frac{n}{(n^2+2)^2} \frac{k_{max} W_{1/2}}{f} \quad (25)$$

where n is the refractive index $=1.773$ [19], $W_{1/2}$ the halfwidth of the band, $7400\,cm^{-1}$, k_{max} the absorption coefficient at the maximum, $0.63\,cm^{-1}$,

and f the oscillator strength. Use of $c_{Ni^{3+}} \cong 2.7 \times 10^{17}\,cm^{-3}$ leads to $f = 1.25 \times 10^{-2}$. A different formula used by Tippins [8]

$$\frac{c}{cm^{-3}} = 1.786 \times 10^{12} k_{max} W_{1/2}/f \quad (26)$$

gives $f = 3.07 \times 10^{-2}$. The value of f is intermediate between what is expected for an allowed transition ($f \cong 1$) and for a forbidden transition. This leaves open both possibilities for the attribution of the absorption band: an internal crystal field transition in the Ni^{3+} ion, or a transfer transition from the valence band to the empty Ni'_{Al} level. The isotherm of absorption strength shown in Fig. 5 has the theoretical shape at $p_{O_2} > 10^{-2}$ Pa but is steeper than expected from the high temperature situation at lower p_{O_2}.

A similar effect was observed in Al_2O_3: Mg [9] and was attributed there to the presence of donors with a level above the acceptor level, but close enough for it to be occupied by electrons at high temperature to an extent sufficient to accept holes from the Mg'_{Al} acceptor level upon cooling. In that case the donor was found to be iron, Fe^{x}_{Al}. The same element is probably responsible for the effect here, the trapping of $\cong 5 \times 10^{16}\,cm^{-3}$ holes required to explain the cut-off can easily occur at the $8.1 \times 10^{17}\,cm^{-3}$ iron atoms present in the sample when the Fe^{x}_{Al} level is slightly above the Ni'_{Al} level as assumed in [1].

5. Conclusion

Measurements of electrical conductivity combined with emf measurements of partially compensated Al_2O_3 containing iron, nickel and magnesium show that nickel, substituting for aluminium, is an acceptor with a level 2.46 eV above the valence band if a large polaron model applies, 2.57 eV $- H(\mu_h)$ above the valence band if a small polaron model applies. Nickel is present as Ni^{2+} at low, as Ni^{3+} at high oxygen pressure, the two species having equal concentrations at $p_{O_2} = 10^{-1}$ Pa. Ni^{3+} gives rise to an absorption band with a maximum at 420 nm with an oscillator strength $f = (1.3$ to $3) \times 10^{-2}$, indicating that the transition is either a transfer transition or an internal, crystal field transition. The native defect compensating Ni'_{Al} is $V_O^{2\cdot}$, $Al_i^{3\cdot}$ being a minority species. The enthalpies of Frenkel and Schottky disorder are related through $H_{F,Al} - \frac{1}{2}H_S = 121\,kJ\,mol^{-1}$. Values of the enthalpy of $V_O^{2\cdot}$ destruction with formation of holes, $H_{ox,V(O)}$ vary from 524 to 700 kJ mol^{-1} (small polaron model) or 900 kJ mol^{-1} (large polaron model). Hole mobility at 1500° C is $1.4 \times 10^{-2}\,cm^2\,V^{-1}\,sec^{-1}$ for the large polaron model, $4.3 \times 10^{-7}\,cm^2\,V^{-1}\,sec^{-1}$ for the small polaron model.

Acknowledgement

Support by the US Department of Energy under Contract No. AS03–76 SF 001113 Project Agreement AT03–76 Er 71027, is gratefully acknowledged.

References

1. F. A. KRÖGER, *Solid State Ionics* **12** (1984) 189.
2. S. A. MARSHALL, *Bull. Am. Phys. Soc.* **5** (1960) 158.
3. S. A. MARSHALL, T. T. KIKUCHI and A. R. REINBERG, *Phys. Rev.* **125** (1962) 453.
4. S. GESCHWIND and J. P. REMEIKA, *J. Appl. Phys.* **33** (1962) 370.
5. R. MÜLLER and HS. H. GÜNTHARD, *J. Chem. Phys.* **44** (1966) 365.
6. D. S. McCLURE, *ibid.* **36** (1962) 2757.
7. K. C. RADFORD and P. L. PRATT, *Proc. Brit. Ceram. Soc.* **15** (1970) 185.
8. H. H. TIPPINS, *Phys. Rev. B* **1** (1970) 126.
9. H. A. WANG, C. H. LEE, F. A. KRÖGER and R. T. COX, *ibid.* **27** (1983) 3821.
10. C. H. LEE and F. A. KRÖGER, *J. Amer. Ceram. Soc.* in press.
11. M. M. EL-AIAT, L. D. HOU, S. K. TIKU, H. A. WANG and F. A. KRÖGER, *ibid.* **64** (1981) 174.
12. P. ODIER, J. C. RIFFLET and J. P. LOUP, *J. Mater. Sci.* **19** (1984) 2121.
13. G. J. DIENES, D. O. WELCH, C. R. FISHER, R. D. HATCHER, O. LAZARETH and M. SAMBERG, *Phys. Rev. B* **11** (1975) 3060.
14. C. R. A. CATLOW, R. JAMES, M. C. MACKRODT and R. F. STEWART, *ibid.* **25** (1982) 1006.
15. B. V. DUTT, J. P. HURRELL and F. A. KRÖGER, *J. Amer. Ceram. Soc.* **58** (1975) 420.
16. S. K. TIKU and F. A. KRÖGER, *ibid.* **63** (1980) 31.
17. S. K. MOHAPATRA, S. K. TIKU and F. A. KRÖGER, *ibid.* **62** (1979) 50.
18. D. L. DEXTER, *Phys. Rev.* **101** (1956) 48.
19. Critical Tables.

Received 1 October
and accepted 15 October 1984